Inadequacy of Third-Order Elastic Coefficients for Predicting Nonlinearity in Highly n-Type-Doped Silicon Resonators

Beheshte Khazaeili and Reza Abdolvand

***Abstract*— Third-order nonlinear elastic coefficients of silicon have been assumed to be the dominant factor in describing the nonlinear behavior of silicon-based resonators in literature. In this article, it is postulated that in spite of the common belief, third-order elastic coefficients may not be adequate to explain the nonlinear elastic behavior of silicon micro-resonators at high n-type doping concentrations. The nonlinear behavior observed in degenerately n-type-doped bulk-extensional mode resonators aligned to ⟨100⟩ orientation is carefully studied in which a spring-hardening effect is observed at large vibration amplitudes. It is shown that the existing analytical/numerical calculations and a proposed finite element model that are based on the utilization of third-order elastic (TOE) coefficients will all predict spring-softening in such resonators, thus suggesting insufficiency of the nonlinear model.**

***Index Terms*— Duffing nonlinearity, nonlinearity, resonators.**

I. Introduction

SILICON-BASED microelectromechanical systems (MEMS) oscillators, which have become widely available in recent years, offer a cost and package-size advantage over the historically dominant quartz technology. However, reducing the resonator size results in higher energy density, and consequently, lower power handling capability. On the other hand, while a small size is essential in today's applications, any compromise in performance, such as signal to noise ratio, cannot be tolerated. In order to satisfy such demanding specifications, the resonators should be excited at relatively large vibration amplitudes, and hence, operation outside the linear regime is expected. For example, in modern data and wireless communication applications, it is challenging to obtain sufficient phase noise performance using the micro-resonator-based oscillators due to their limited linear dynamic range [1], [2]. Therefore, to increase their energy storage, and consequently, the signal to noise ratio, these resonators should be run near to their nonlinear operational area [2], [3]. In addition, when micro-resonators are used as high-resolution sensors, such as Atto-Newton force sensor [4], electronic spin detector [5], or zepto-scale mass sensor [6], large signal to noise ratio [7] and low phase noise [8] are critical requirements. For meeting these criteria, the MEMS oscillator amplitude should be set to large values while avoiding excessive nonlinearity [9]. As a specific example, in a MEMS gyroscope, the sensitivity of the device is directly proportional to the resonator amplitude of vibration, which, in turn, is limited by nonlinearity [10].

Herewith, nonlinear models that could comprehensively capture the behavior of silicon micro-resonators are sought-after. Nonlinearity in silicon-based resonators has been studied in the past. Material nonlinearity [2], [11], [12], geometric nonlinearity [2], [11]–[13], and electrostatic nonlinearity [2], [9], [12] are some of the underlying mechanisms identified for explaining the nonlinear behavior depending on the regime of operation and the transduction mechanism utilized. Design techniques to reduce the nonlinear behavior of silicon resonators have also been widely explored [14]–[17]. Regardless of the resonator type, an accurate estimation of the nonlinear elastic coefficients of silicon is essential for developing a model that estimates the nonlinear behavior in this kind of device. Recent experimental studies have revealed that nonlinearity in silicon resonators is a sensitive function of the doping type and concentration [12], [17]. However, a direct connection between nonlinear elastic properties of doped silicon and resonator nonlinearity is yet to be established. It is currently believed in the MEMS community that the third-order nonlinear elastic coefficients are sufficient for predicting the nonlinearity of silicon [2], [11], [18], [19]. Both numerical [11] and closed-form analytical [18] methods for finding nonlinear Young's modulus and consequently nonlinear amplitude-frequency coefficient have been proposed based on the third-order nonlinear constitutive equation of silicon assuming that the effect of higher order nonlinearities are negligible. In this article, this assumption is put to the test for the specific case of highly doped n-type ⟨100⟩ silicon, and it is postulated that nonlinear coefficients beyond third-order are required.

II. Theory of Nonlinearity

A modified equation of motion for a nonlinear lumped mass-spring-damper system can be used to represent a nonlinear

Manuscript received September 29, 2019; revised November 27, 2019; accepted December 17, 2019. Date of publication January 16, 2020; date of current version January 27, 2020. This work was supported by the NSF under Award 1711632. The review of this article was arranged by Editor S. Hong. *(Corresponding author: Beheshte Khazaeili.)*

The authors are with the Department of Electrical and Computer Engineering, University of Central Florida, Orlando, FL 32816 USA (e-mail: beheshteh.khazaeili@knights.ucf.edu; reza.abdolvand@ucf.edu).

Color versions of one or more of the figures in this article are available online at http://ieeexplore.ieee.org.

Digital Object Identifier 10.1109/TED.2019.2961946

MEMS resonator response

$$m\ddot{x} + c\dot{x} + k(x)x = F\cos(\omega t) \tag{1}$$

in which x, c, m, F, and ω represent modal displacement, linear damping coefficient, effective mass, amplitude, and frequency of the external force applied to the system, respectively. $k(x)$ is the amplitude-dependent stiffness coefficient, which is usually represented by a second-order polynomial as (2)

$$k(x) = k_0 + k_1 x + k_2 x^2 \tag{2}$$

where k_0, k_1, and k_2 are the linear, first- and second-order nonlinear spring constants. The resonance frequency of such a system is a function of vibration amplitude (a) as follows [12]:

$$f = f_0(1 + Ka^2), \quad K = \frac{3}{8}\frac{k_2}{k_0} - \frac{5}{12}\frac{k_1^2}{k_0^2} \tag{3}$$

where f_0 is the initial resonance frequency, and K is the amplitude-frequency (A-f) coefficient. For a silicon-based resonator with lateral-extensional (i.e., contour) mode shape, linear/nonlinear spring stiffness coefficients are a function of resonator dimensions and nonlinear Young's modulus [20], as shown in (4)

$$k_0 = \frac{\pi^2 E_0 A_0}{2L}, \quad k_1 = \frac{4\pi^2 E_1 A_0}{3L^2}, \quad k_2 = \frac{3\pi^4 E_2 A_0}{8L^3} \tag{4}$$

in which A_0 and L are the undeformed cross-sectional area and dimension (either length or width) of the resonator along which the lateral-extensional mode shape happens. In addition, E_0, E_1, and E_2 are the linear, first-, and second-order nonlinear Young's modulus coefficients in the nonlinear equation of Young's modulus, which is defined as the ratio of engineering stress (T) to engineering strain (S)

$$E = \frac{T}{S} = E_0 + E_1 S + E_2 S^2. \tag{5}$$

Nonlinear Young's modulus coefficients are typically calculated based on second-order linear and third-order nonlinear elastic stiffness constants starting from the nonlinear stress-strain constitutive equation for silicon. Equation (6) shows the Cauchy stress (σ) as a function of Lagrangian strain (η) when both geometric and material nonlinearity is considered [11]

$$\sigma_{ij}(X) = \frac{\rho_X}{\rho_\alpha}\frac{\partial X_i}{\partial \alpha_k}\frac{\partial X_j}{\partial \alpha_k}(C_{ijkl}\eta_{kl} + C_{ijklmn}\eta_{kl}\eta_{mn}) \tag{6}$$

where ρ_X and ρ_α represent the deformed and undeformed densities. In addition, X is the particle coordinate at the finite deformation, and α is the undeformed state. C_{ijkl} and C_{ijklmn} are the second- and third-order elastic (TOE) stiffness coefficients of an anisotropic material (silicon in our case), respectively.

III. Nonlinearity Modeling in a Silicon Resonator

Using the methods described below, we attempt to predict the nonlinear behavior of a bulk-extensional silicon-based resonator fabricated on a highly doped n-type substrate (n∼5e19 cm^{-3}). The resonator is a thin-film piezoelectric on silicon (TPoS) resonator [21] fabricated on a silicon-on-insulator (SOI) wafer with an 8-μm thick ⟨100⟩ silicon device layer. The piezoelectric material in this device is a 0.5-μm thick aluminum nitride (AlN) layer sandwiched between two 100-nm thick molybdenum layers used as top and bottom electrodes. Fig. 1(a) and (b) show the schematic and the scanning electron micrograph (SEM) of the device, respectively.

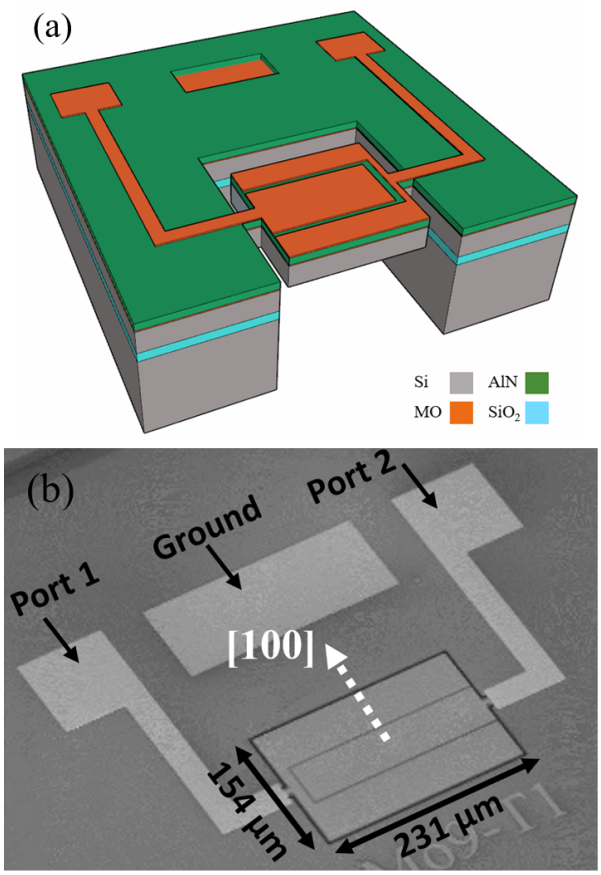

Fig. 1. (a) Schema of TPoS resonator and (b) SEM image of the device.

Resonators are designed and fabricated to be aligned to either ⟨100⟩ or ⟨110⟩ planes. The fundamental lateral-extensional (i.e., contour) resonance mode of the block resonators is actuated using a two-port electrode configuration, as seen in Fig. 1.

By using both methods described in [11] and [18], the linear and nonlinear Young's modulus coefficients and A-f coefficient (K) are calculated for the ⟨100⟩-aligned bulk-extensional resonator with dimensions of 231 × 154 × 8 (μm)^3 shown in Fig. 1. The second- and TOE coefficients for highly doped n-type silicon (n∼2e19 cm^{-3}) found in [22] are used for the calculations presented in the next sections.

A. Numerical Method to Find Nonlinear Young's Modulus

For finding nonlinear Young's modulus, one method is to solve (6) based on numerical solutions as a function of applied stress and then convert Cauchy stress and Lagrangian strain to engineering stress and strain as follows [11]:

$$T_{ii} = \left(\frac{\partial X_i}{\partial \alpha_i}\right)^2 \sigma_{ii}, \quad S_{ii} = \frac{\partial X_i}{\partial \alpha_i} - 1. \tag{7}$$

By fitting the obtained engineering stress and strain values to (5), nonlinear Young's modulus coefficients are found as $E_0 = 127.3$ GPa, $E_1 = 221.7$ GPa, and $E_2 = -602.2$ GPa.

Now, by substituting these values along with $L = 154\ \mu$m and $A_0 = 231 \times 8\ (\mu\text{m})^2$ in (4), linear and nonlinear spring stiffness constants of our device are found as $k_0 = 7.53\text{e}6\ \text{Pa}\cdot\text{m}$, $k_1 = 2.27\text{e}11$ Pa, $k_2 = -1.1\text{e}16\ \text{Pa}\cdot\text{m}^{-1}$.

Therefore, the A-f coefficient K is calculated using (3)

$$K = \frac{3}{8}\frac{k_2}{k_0} - \frac{5}{12}\frac{k_1^2}{k_0^2} = -9.33e8\ \text{m}^{-2}.$$

As seen, a negative K is obtained. According to amplitude-dependent resonance frequency (3), the negative sign of K means that the resonance frequency of the device decreases by increasing the amplitude of vibration a (i.e., spring softening).

B. Closed-Form Equation to Find Nonlinear Young's Modulus

Besides the numerical solution proposed by Kaajakari *et al.* [11] and Kim and Sachse [18] have proposed a closed-form equation for nonlinear Young's modulus coefficients as a complicated function of linear and nonlinear elastic stiffness constants. For notational simplicity, some unit-less parameters are defined as follows [18]:

$$\nu_0 \equiv \frac{c_{12}}{c_{12}+c_{11}} \tag{8}$$

$$h_1 \equiv \frac{c_{112}}{2c_{12}} \quad h_2 \equiv \frac{c_{112}+c_{123}}{c_{11}+c_{12}} \quad h_3 \equiv \frac{c_{111}+3c_{112}}{2(c_{11}+c_{12})} \tag{9}$$

$$g_1 \equiv h_1 - h_2 + \nu_0 h_3 \tag{10}$$

$$g_2 \equiv h_2^2 - h_1 h_2 + \nu_0 h_3(2h_1 - 3h_2) + 2\nu_0^2 h_3^2 \tag{11}$$

$$E_0 \equiv c_{11} - 2\nu_0 c_{12} \tag{12}$$

$$e_1 \equiv E_0(1+2\nu_0) + c_{12}\left(\nu_0^{-1}h_3 - 3h_1 - 6\nu_0 h_1 + 3\nu_0 h_2 - 2\nu_0^2 h_3\right) \tag{13}$$

$$e_2 \equiv E_0\left(2\nu_0 + 4\nu_0^2 + 2\nu_0 g_1 - 0.5\right) + c_{12}\Big[\left(\nu_0^{-1}+2\right) \times \left(h_3 - 3\nu_0 h_1 - 6\nu_0^2 h_1 + 3\nu_0^2 h_2 - 2\nu_0^3 h_3\right) - 2\nu_0(2h_1 g_1 - h_2 g_1 + g_2)\Big]. \tag{14}$$

At a stress-free natural state, E_0 and ν_0 represent Young's modulus and Poisson's ratio of a cubic material. Nonlinear engineering Young's modulus coefficients in (5) can be calculated as [18]

$$E_1 = \frac{1}{2}E_0 - 2\nu_0 E_0 + e_1 \tag{15}$$

$$E_2 = -2\nu_0 E_0 - 2\nu_0 g_1 E_0 + e_1 - 2\nu_0 e_1 + e_2. \tag{16}$$

Using the elastic coefficients in [22], Young's modulus coefficients and consequently spring stiffness constants and A-f coefficient are calculated as $E_0 = 127.3$ GPa, $E_1 = 237.3$ GPa, $E_2 = -656.8$ GPa, $k_0 = 7.5\text{e}6\ \text{Pa}\cdot\text{m}$, $k_1 = 2.4\text{e}11$ Pa, $k_2 = -1.2\text{e}16\ \text{Pa}\cdot\text{m}^{-1}$, $K = -1.038\text{e}9\ \text{m}^{-2}$.

In both numerical and closed-form equation methods, second-order linear and third-order nonlinear elastic stiffness coefficients are considered assuming that higher order nonlinear elastic constants are negligible in silicon.

As calculated above, a negative E_2, and consequently, a negative K (i.e., spring-softening) is predicted using both numerical and closed-form methods. This predicted trend for the lateral extensional mode of a ⟨100⟩-aligned silicon-based resonator is exactly the opposite of the observed spring-hardening measured by our group and others [12], [17].

One can argue that the discrepancy might be due to using elastic constants of phosphorus-doped silicon with a doping concentration of n∼2e19 cm^{-3}, while the measurement results are for phosphorus-doped silicon with a doping concentration of n∼5e19 cm^{-3}. It should be noted that among all available reported silicon elastic constants in literature, 2e19 cm^{-3} is the closest doping concentration to our experiment. In addition, error in measuring the elastic constants of silicon reported in [22] could possibly be assumed as another cause of the discrepancy. In order to investigate the possibility of this source of error, different tolerance ranges of ±400%, ±250%, and ±120% each with 700 steps were considered for the reported elastic constants C_{111}, C_{112}, and C_{123}. Then, K was recalculated for each combination of those values using closed-form equations for Young's modulus. However, none of the altered elastic constants resulted in a positive K, therefore, this possible source of error was eliminated.

In addition, self-heating of the resonator was ruled out as the source of the observed spring-hardening effect in measurement, as the temperature coefficient of resonance frequency (TCF) of these devices are either close to zero (the device was checked at turnover temperature) or negative where any thermal shift would result in softening.

This discrepancy may also reasonably be associated with the approximations made for simplification of the analysis, such as a 2-D stress approximation (the stress is assumed to be uniform along the length). To investigate this possible source of error and validate the previous calculations, a novel finite element 3-D model to predict nonlinearity of the resonator is developed and presented in the next section.

C. Proposed 3-D Numerical Model to Predict Nonlinearity

In this model, the anisotropic material elasticity matrix is modified to be strain-dependent. The nonlinear relation between second Piola-Kirchhoff stress (τ) and Lagrangian strain (η) is described as [11], [18]

$$\tau_{ij} = C_{ijkl}\eta_{kl} + \frac{1}{2}C_{ijklmn}\eta_{kl}\eta_{mn}. \tag{17}$$

Equation (17) can be rewritten as follows:

$$\tau_{ij} = (C_{ijkl} + \frac{1}{2}C_{ijklmn}\eta_{mn})\eta_{kl}. \tag{18}$$

The expression in parentheses is then redefined as a new elastic stiffness tensor

$$C'_{ijkl} = C_{ijkl} + \frac{1}{2}C_{ijklmn}\eta_{mn} \quad i,j,k,l,m,n = 1,2,3. \tag{19}$$

In fact, the linear second-order elastic (SOE) stiffness tensor can be modified so that it is strain-dependent with the coefficient of nonlinear elastic constants. Voigt notation is then used to convert the equation from tensor to matrix format. The same relationship presented in (18) and (19) is shown in (20) but in

a matrix format

$$\tau_i = \left(C_{ij} + \frac{1}{2}C_{ijk}\eta_k\right)\eta_j$$
$$C'_{ij} = C_{ij} + \frac{1}{2}C_{ijk}\eta_k \quad i, j, k = 1, 2, 3, 4, 5, 6. \tag{20}$$

Now using Einstein notation and considering cubic symmetry for a silicon crystalline structure, the above equation can be expanded to find all of 36 components of the new modified stiffness matrix C'_{ij}.

Silicon has cubic symmetry which requires three independent SOE constants

$$C_{11} = C_{22} = C_{33} = 163.94 \text{ GPa}$$
$$C_{12} = C_{13} = C_{23} = 64.77 \text{ GPa}$$
$$C_{44} = C_{55} = C_{66} = 79.19 \text{ GPa} \tag{21}$$

and six independent TOE constants [18]

$$C_{111} = C_{222} = C_{333} = -658 \text{ GPa}$$
$$C_{112} = C_{223} = C_{133} = C_{113} = C_{122} = C_{233} = -511 \text{ GPa}$$
$$C_{144} = C_{255} = C_{366} = 65 \text{ GPa}$$
$$C_{155} = C_{244} = C_{344} = C_{166} = C_{266} = C_{355} = -336 \text{ GPa}$$
$$C_{123} = 60 \text{ GPa}$$
$$C_{456} = -86 \text{ GPa}. \tag{22}$$

Values of second and third-order stiffness constants for highly doped n-type (n$\sim$2e19 cm^{-3}) silicon are found in the literature [22].

Considering this symmetry and (20), linear elasticity matrix C (or sometimes noted as D) for silicon can be modified as follows in COMSOL:

$$C' = \begin{bmatrix} C'_{11} & C'_{12} & \cdot & \cdot & \cdot & C'_{16} \\ \cdot & \cdot & & & & \cdot \\ \cdot & & \cdot & & & \cdot \\ \cdot & & & \cdot & & \cdot \\ \cdot & & & & \cdot & \cdot \\ C'_{61} & \cdot & \cdot & \cdot & \cdot & C'_{66} \end{bmatrix} \tag{23}$$

where C'_{ij} is the modified strain-dependent elastic constant that can be calculated as

$$C'_{11} = C_{11} + \frac{1}{2}C_{111}\eta_1 + \frac{1}{2}C_{112}\eta_2 + \frac{1}{2}C_{113}\eta_3$$
$$C'_{12} = C_{12} + \frac{1}{2}C_{121}\eta_1 + \frac{1}{2}C_{122}\eta_2 + \frac{1}{2}C_{123}\eta_3$$
$$\vdots$$
$$C'_{14} = \frac{1}{2}C_{144}\eta_4$$
$$C'_{66} = C_{66} + \frac{1}{2}C_{166}\eta_1 + \frac{1}{2}C_{266}\eta_2 + \frac{1}{2}C_{366}\eta_3. \tag{24}$$

Strain $\eta_i = 1, 2, 3, 4, 5, 6$ mentioned in the above equation is defined as elastic strain tensor (solid.eelij i, j = 1, 2, 3) in COMSOL. Voigt notation is used for this conversion as, η_1 = solid.eel11, η_2 = solid.eel22, η_3 = solid.eel33, η_4 = solid.eel23, η_5 = solid.eel13, η_6 = solid.eel12.

It should be noted that in order to correctly model the nonlinear behavior of the device, both geometric and material nonlinearities should be considered. Geometric nonlinearity is a predefined option in COMSOL and can be easily included. Once chosen, engineering stress and strain definitions are not valid as small deformation approximations lose accuracy, and they will be replaced by second Piola-Kirchhoff stress and Lagrangian strain definitions. More details regarding geometric nonlinearity can be found in [13]. For verifying the effectiveness of the predefined geometric nonlinearity option in COMSOL, the nonlinear behavior of the fundamental flexural-mode of a clamped-clamped beam is simulated using the proposed 3-D model (Fig. 2). It is known in the literature that for this mode, geometric nonlinearity is dominant and causes spring hardening amplitude-frequency nonlinear behavior [23], [24]. Fig. 2(a) shows the first in-plane mode-shape of the fixed-fixed beam made from highly doped n-type silicon when material nonlinearity of silicon was defined as explained above and predefined geometric nonlinearity option in COMSOL was also included.

In order to characterize the amplitude-frequency nonlinearity of the beam, a ringdown test [9] is simulated. The beam is excited with an alternating force signal for a set period of time in time-domain, and the decaying vibration amplitude is analyzed after the signal is ceased. The decaying waveform is divided into several bins, and fast Fourier transform (FFT) is applied to find the change of resonance frequency with amplitude. This concept is shown in Fig. 2. The COMSOL model of the beam, which is excited with the pulse modulated sinusoidal force at resonance, is depicted in Fig. 2(a). The simulated decaying signal is shown in Fig. 2(b) and the zoomed-in view of some of the bins in the decaying signal and their corresponding FFT are shown in Fig. 2(c) and (d) to demonstrate how the resonance frequency is shifting with the amplitude of vibration. As seen, the resonance frequency of the beam is maximum for the first bin with the maximum amplitude of vibration and starts to decrease over the decaying signal. This hardening behavior is best represented by the so-called *backbone curve*, which is the normalized resonance frequency shift for different amplitudes of vibration, as shown in Fig. 2(e). The predicted hardening nonlinearity for the beam agrees with theory and confirms the effectiveness of the predefined geometric nonlinearity option in COMSOL.

After confirming that both geometric and material nonlinearity could be properly defined in our finite element model (FEM), simulation of the nonlinear behavior in the extensional-mode ⟨100⟩ silicon resonator is now attempted. In order to do so, the same ringdown method that was explained above for the beam simulation is employed.

The resonator is simply modeled as a block of silicon with the same dimensions as the fabricated device shown in Fig. 3(a). The ringdown signal and backbone curve for the simulated resonator are shown in Fig. 3(b) and (c), respectively. As seen, our proposed 3-D model also predicts spring softening for this device which is consistent with previous numerical and analytical solutions.

It is worth noting that in modeling nonlinearity of the resonator in Fig. 3(a) with a pure silicon block, the assumption is that the silicon body dominates the nonlinear properties of the TPOS resonator under study. The justification for the validity of this assumption is twofold. First, devices with the

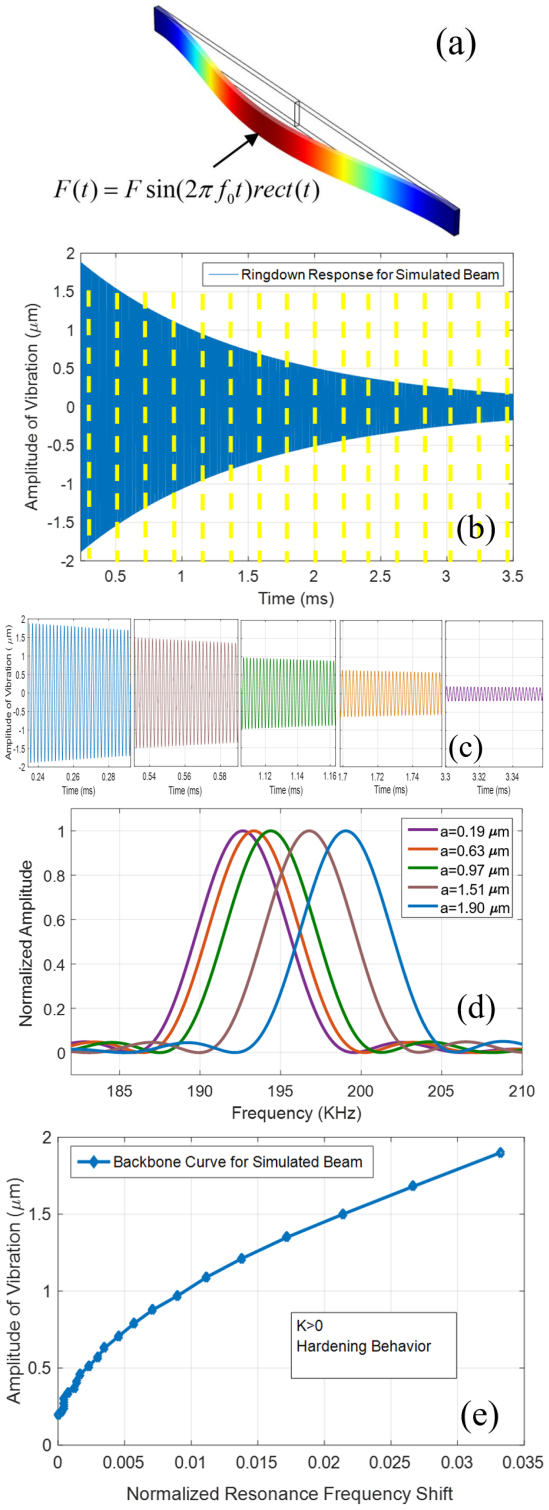

Fig. 2. Proposed FEM model and ringdown method for simulation of amplitude-frequency nonlinearity. (a) Clamped-clamped beam COMSOL model, (b) ringdown response, (c) zoomed-in view of some of the bins in the ringdown response, (d) corresponding FFTs of these bins, and (e) obtained backbone curve for the simulated beam. Predicted hardening for the clamped-clamped beam confirms the effectiveness of the predefined geometric nonlinearity option in COMSOL.

exact same design fabricated on the same wafer but aligned to ⟨110⟩ crystalline orientation of silicon show completely different nonlinear behavior compared to those aligned to ⟨100⟩

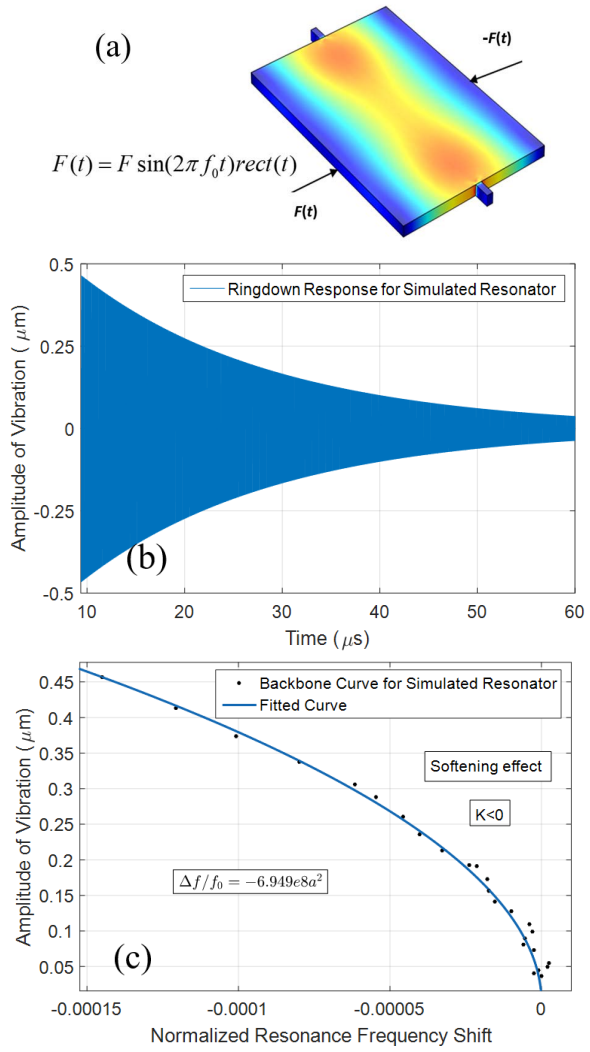

Fig. 3. (a) COMSOL model, (b) simulation results for the ringdown response, and (c) corresponding backbone curve for the resonator under study. Spring softening is predicted.

(softening behavior for resonators aligned to ⟨110⟩ versus hardening behavior for those aligned to ⟨100⟩) [17], [25]. If the dominant layer in determining the amplitude-frequency nonlinearity of our device was any layer other than silicon, the same nonlinear behavior should have been observed for both orientations since all other layers (i.e., sputtered AlN and molybdenum) are isotropic in the *XY* plane. Second, other groups have also reported similar spring hardening/softening behavior for their pure-silicon capacitive lateral extensional resonators fabricated on degenerately n-type-doped silicon and aligned to ⟨100⟩/⟨110⟩, respectively [12].

IV. Measurement Results

The frequency response of the resonator under study for varying input powers is presented in Fig. 4(a). As seen, spring hardening is observed for the device from which a positive A-f coefficient could be concluded opposing the presented analytical and simulated results earlier. In order to estimate *K* for the measured resonator, a method previously developed in our group is utilized [25], [33]. S-parameters of the device for

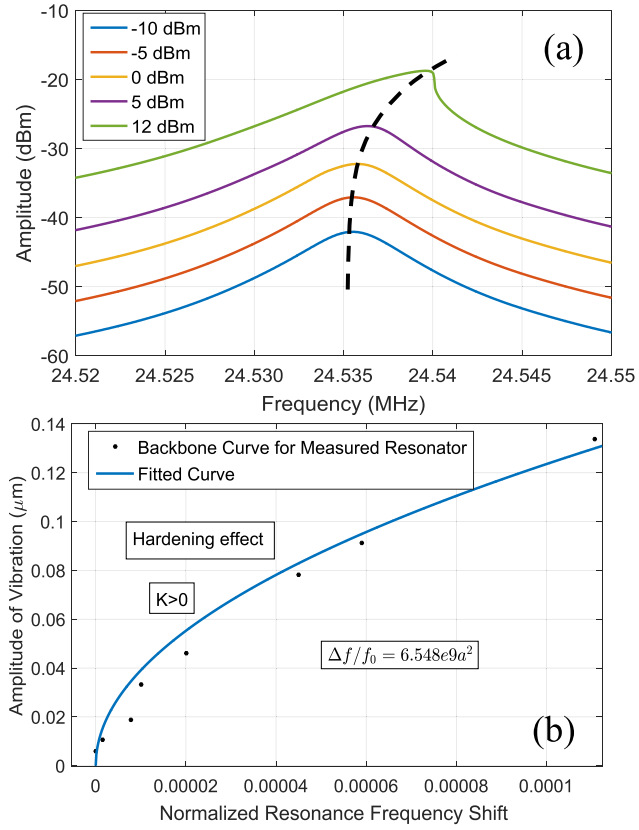

Fig. 4. (a) Measured output voltage amplitude for varying input amplitudes applied to a TPoS resonator with 8-μm silicon and 0.5-μm AlN aligned to the <100> silicon crystalline plane and (b) backbone curve derived from the measurement. Spring hardening is observed.

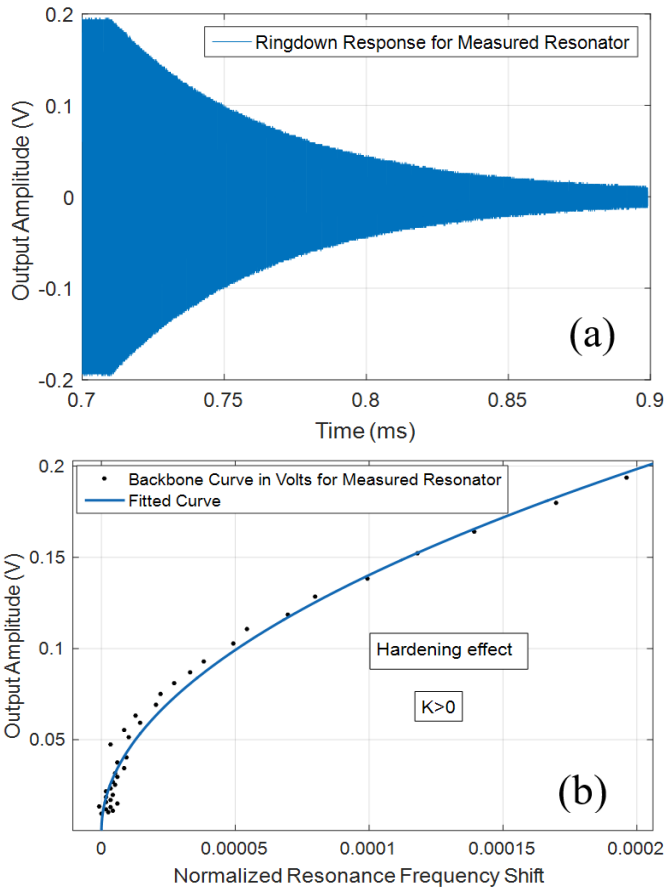

Fig. 5. (a) Measurement results for the ringdown response and (b) corresponding backbone curve in volts for the resonator under study. Spring hardening is observed.

several input powers are measured using a network analyzer and imported to Advanced Design Systems (ADS) software, and the amplitude of vibration for each specific input voltage is calculated. In this approach, the resonator is modeled by a two-port network in which S-parameters of the resonator are embedded. In addition, the network analyzer 50-Ω terminations and the input voltage source are also modeled in ADS. By using this equivalent circuit, the phase and magnitude of the input and output current/voltage of the resonator are extracted. With this information, energy stored in the device, and consequently, the amplitude of vibration is calculated for each input power.

The normalized resonance frequency shift of the device measured by the network analyzer for each input power is then plotted versus the corresponding calculated amplitude of vibration. The obtained backbone curve is then fit with (3) to estimate $K = 6.548\text{e}9\ \text{m}^{-2}$ [Fig. 4(b)]. The results attained from the frequency response measurement presented above are then further confirmed with the same ringdown measurement method explained in the simulation section. The measured decaying signal and the backbone curve in volts are shown in Fig. 5(a) and (b). As seen, spring hardening behavior is clearly observed in this case again.

V. Discussion

It was shown that all the existing and proposed models fail to predict the measured mechanical nonlinearity in highly doped n-type bulk-extensional resonators. Table I shows the calculated K values for the resonator under study obtained from different methods explained in the previous sections. As seen, all existing and proposed models predict a negative K (spring softening), which is completely opposite to the positive K (spring hardening) obtained from measurement. This indicates a fundamental insufficiency in all the above methods, including the numerical solution, closed-form equation, and presented a 3-D simulation model.

We believe that this discrepancy is due to the assumption that fourth-order stiffness elastic constants of silicon have a negligible effect. Considering that the TOE constants do not

TABLE I
Amplitude-Frequency Coefficient K

	E_0 (GPa)	E_1 (GPa)	E_2 (GPa)	A-f coefficient K (1/m²)
Experiment	NA	NA	NA	+6.548e9
Proposed FEM model	NA	NA	NA	-6.949e8
Method in [11]	127.3	221.7	-602.2	-9.332e8
Method in [18]	127.3	237.3	-656.8	-1.038e9

appear to be the dominant factor in the nonlinear behavior of the studied resonators, this hypothesis is plausible.

Unfortunately, there is no data on such higher order stiffness elastic constants of silicon, so we cannot take them into account in the above-mentioned models to confirm our hypothesis.

However, there are some prior publications studying the material properties of silicon at high pressures that support our hypothesis about the insufficiency of TOE constants of silicon for predicting its nonlinear behavior. For example, in [26], the phase transition of cubic-to-tetragonal for group IV semiconductors at high pressures is studied based on Landau theory. The utilized theoretical approach in this article to effectively explain such phenomena is equivalent to considering a higher order (at least fourth-order) elastic nonlinearity [26].

In addition, it is worth noting that the most common method used in literature to measure nonlinear TOE constants of a material is through measuring the phase velocity of a sound wave, exposed to the stressed targeted media. The measured velocities at different applied stresses are then fit by the theoretical formulas that were developed to predict the sound wave velocity in the nonlinear media where only up to TOE constants are taken into account [27]–[31].

It is concluded in [19] that the measured precursor velocity in ⟨110⟩ and ⟨111⟩ silicon is in good agreement with third-order theory proposed by Holt and Ford [27] and Holt [30] confirming negligibility of fourth-order elastic constants for these orientations. However, for ⟨100⟩ silicon, the measurement results do not completely match with the third-order theory, which suggests the inadequacy of TOE constants in predicting the nonlinear behavior of silicon in ⟨100⟩ orientation. This is also the case for quartz, where [32] showed that it is necessary to consider the fourth-order elastic nonlinearity for quartz. In this article, we argue that the same situation exists for silicon at least for ⟨100⟩ crystalline plane.

VI. Conclusion

In this article, it is demonstrated that the two existing theoretical methods and the proposed FEM, cannot correctly predict amplitude-frequency nonlinear behavior of a lateral-extensional highly doped n-type silicon block resonator. Several common possibilities, such as 2-D approximation and self-heating, are ruled out as the cause of this discrepancy, and higher order (fourth and higher) nonlinearities in silicon are postulated as the most probable cause. Considering technology improvements in the last decades, the authors believe that accurate measurement of higher order material nonlinearities, including third- and fourth-order elastic constants of silicon at different doping types and concentrations, will definitely assist researchers in a variety of disciplines, and specifically, the MEMS community.

References

[1] T. Mattila *et al.*, "A 12 MHz micromechanical bulk acoustic mode oscillator," *Sens. Actuators A, Phys.*, vol. 101, nos. 1–2, pp. 1–9, Sep. 2002.

[2] V. Kaajakari, T. Mattila, A. Oja, and H. Seppa, "Nonlinear limits for single-crystal silicon microresonators," *J. Microelectromech. Syst.*, vol. 13, no. 5, pp. 715–724, Oct. 2004.

[3] R. M. C. Mestrom, R. H. B. Fey, J. T. M. van Beek, K. L. Phan, and H. Nijmeijer, "Nonlinear oscillation in MEMS resonators," *Sens. Actuators A, Phys.*, vol. 142, no. 1, pp. 306–315, 2008.

[4] T. D. Stowe, K. Yasumura, T. W. Kenny, D. Botkin, K. Wago, and D. Rugar, "Attonewton force detection using ultrathin silicon cantilevers," *Appl. Phys. Lett.*, vol. 71, no. 2, pp. 288–290, Jul. 1997.

[5] D. Rugar, R. Budakian, H. J. Mamin, and B. W. Chui, "Single spin detection by magnetic resonance force microscopy," *Nature*, vol. 430, no. 6997, pp. 329–332, 2004.

[6] Y. T. Yang, C. Callegari, X. L. Feng, K. L. Ekinci, and M. L. Roukes, "Zeptogram-scale nanomechanical mass sensing," *Nano Lett.*, vol. 6, no. 4, pp. 583–586, Apr. 2006.

[7] M. Agarwal *et al.*, "Scaling of amplitude-frequency-dependence nonlinearities in electrostatically transduced microresonators," *J. Appl. Phys.*, vol. 102, no. 7, Oct. 2007, Art. no. 074903.

[8] V. Kaajakari, T. Mattila, A. Oja, J. Kiihamaki, and H. Seppa, "Square–extensional mode single-crystal silicon micromechanical resonator for low-phase-noise oscillator applications," *IEEE Electron Device Lett.*, vol. 25, no. 4, pp. 173–175, Apr. 2004.

[9] P. M. Polunin, Y. Yang, M. I. Dykman, T. W. Kenny, and S. W. Shaw, "Characterization of MEMS resonator nonlinearities using the ringdown response," *J. Microelectromech. Syst.*, vol. 25, no. 2, pp. 297–303, Apr. 2016.

[10] Q. Shin, A. Qiu, Y. Su, and R. Shi, "Nonlinear oscillation characteristics of MEMS resonator," in *Proc. IEEE Int. Conf. Mechtron. Automat.*, Aug. 2010, pp. 1250–1253.

[11] V. Kaajakari, T. Mattila, A. Lipsanen, and A. Oja, "Nonlinear mechanical effects in silicon longitudinal mode beam resonators," *Sens. Actuators A, Phys.*, vol. 120, no. 1, pp. 64–70, Apr. 2005.

[12] Y. Yang *et al.*, "Nonlinearity of degenerately doped bulk-mode silicon MEMS resonators," *J. Microelectromech. Syst.*, vol. 25, no. 5, pp. 859–869, Oct. 2016.

[13] E. S. Babayemi, "Experimental characterization of geometrically nonlinear micromechanical resonators," M.S. thesis, Graduate School, Dept. Mech. Eng., Ohio State Univ., Columbus, OH, USA, 2018.

[14] B. Khazaeili, S. Moradian, S. Shahraini, and R. Abdolvand, "Bulk–extensional silicon resonators aligned to non-major crystalline planes," in *Proc. Joint Conf. IEEE Int. Freq. Control Symp. Eur. Freq. Time Forum (EFTF/IFC)*, Apr. 2019, pp. 1–2.

[15] L. C. Shao, M. Palaniapan, and W. W. Tan, "The nonlinearity cancellation phenomenon in micromechanical resonators," *J. Micromech. Microeng.*, vol. 18, no. 6, Jun. 2008, Art. no. 065014.

[16] M. Ghatge, P. Karri, and R. Tabrizian, "Power-insensitive silicon crystal-cut for amplitude-stable frequency synthesis," in *Proc. IEEE 30th Int. Conf. Micro Electro Mech. Syst. (MEMS)*, Jan. 2017, pp. 76–79.

[17] M. Shahmohammadi, H. Fatemi, and R. Abdolvand, "Nonlinearity reduction in silicon resonators by doping and re-orientation," in *Proc. IEEE 26th Int. Conf. Micro Electro Mech. Syst. (MEMS)*, Jan. 2013, pp. 793–796.

[18] K. Y. Kim and W. Sachse, "Nonlinear elastic equation of state of solids subjected to uniaxial homogeneous loading," *J. Meterials Sci.*, vol. 35, no. 13, pp. 3197–3205, 2000.

[19] W. H. Gust and E. B. Royce, "Axial yield strengths and two successive phase transition stresses for crystalline silicon," *J. Appl. Phys.*, vol. 42, no. 5, pp. 1897–1905, Apr. 1971.

[20] Y. Yang *et al.*, "Measurement of the nonlinear elasticity of doped bulk-mode MEMS resonators," in *Proc. Solid-State Sensors, Actuat., Microsyst. Workshop*, Hilton Head Island, SC, USA, Jun. 2014.

[21] R. Abdolvand, H. Lavasani, G. Ho, and F. Ayazi, "Thin-film piezoelectric-on-silicon resonators for high-frequency reference oscillator applications," *IEEE Trans. Ultrason., Ferroelect., Freq. Contr.*, vol. 55, no. 12, pp. 2596–2606, Dec. 2008.

[22] J. J. Hall, "Electronic effects in the elastic constants of n-type silicon," *Phys. Rev.*, vol. 161, no. 3, pp. 756–761, Jul. 2002.

[23] R. Benamar, M. Bennouna, and R. White, "The effects of large vibration amplitudes on the mode shapes and natural frequencies of thin elastic structures, part III: Fully clamped rectangular isotropic plates—Measurements of the mode shape amplitude dependence and the spatial distribution of harmonic distortion," *J. Sound Vib.*, vol. 175, no. 3, pp. 377–395, Aug. 1994.

[24] K. El Bikri, R. Benamar, and M. Bennouna, "Geometrically non-linear free vibrations of clamped-clamped beams with an edge crack," *Comput. Struct.*, vol. 84, no. 7, pp. 485–502, Feb. 2006.

[25] B. Khazaeili, J. Gonzales, and R. Abdolvand, "Acceleration sensitivity in bulk-extensional mode, silicon-based MEMS oscillators," *Micromachines*, vol. 9, no. 5, p. 233, May 2018.
[26] M. Hebbache, "Elastic phase transition in germanium and silicon," *Phys. Rev. B, Condens. Matter*, vol. 49, no. 10, p. 6522, 1994.
[27] A. C. Holt and J. Ford, "Theory of ultrasonic pulse measurements of third-order elastic constants for cubic crystals," *J. Appl. Phys.*, vol. 38, no. 1, pp. 42–50, 1967.
[28] Z.-P. Chang, "Third-order elastic constants of NaCl and KCl single crystals," *Phys. Rev.*, vol. 140, Nov. 1965, Art. no. A1788.
[29] H. J. McSkimin and P. Andreatch, Jr., "Measurement of third-order moduli of silicon and germanium," *J. Appl. Phys.*, vol. 35, no. 11, p. 3312, 1964.
[30] A. C. Holt, "Theory of ultrasonic pulse measurements of third order elastic constants for cubic crystals," Ph.D. dissertation, School Phys., Georgia Inst. Technol., Atlanta, GA, USA, 1967.
[31] R. N. Thurston and K. Brugger, "Third-order elastic constants and the velocity of small amplitude elastic waves in homogeneously stressed media," *Amer. Phys. Soc.*, vol. 135, Sep. 1964, Art. no. AB3.
[32] R. Fowles, "Dynamic compression of quartz," *J. Geophys. Res.*, vol. 72, no. 22, pp. 5729–5742, Nov. 1967.
[33] H. Fatemi and R. Abdolvand, "Fracture limit in thin-film piezoelectric-on-substrate resonators: Silicon vs. diamond," in *Proc. IEEE 26th Int. Conf. Micro Electro Mech. Syst. (MEMS)*, Taipei, Taiwan, Jan. 2013, pp. 461–464.